

Supplementary Materials for Self-assembly of electronically abrupt borophene/organic lateral heterostructures

Xiaolong Liu, Zonghui Wei, Itamar Balla, Andrew J. Mannix, Nathan P. Guisinger, Erik Luijten, Mark C. Hersam

Published 22 February 2017, *Sci. Adv.* **3**, e1602356 (2017)
DOI: 10.1126/sciadv.1602356

The PDF file includes:

- fig. S1. Carpet-mode growth of homogeneous-phase borophene.
- fig. S2. XPS spectra of Ag 3d and O 1s core levels.
- fig. S3. Bias-dependent atomic-resolution images of homogeneous-phase borophene.
- fig. S4. Additional atomic-resolution image of borophene.
- fig. S5. Growth of PTCDA across various interfaces.
- fig. S6. Additional images of PTCDA/borophene lateral heterostructures.
- fig. S7. Design of a coarse-grained model for PTCDA.
- fig. S8. Entropy variation $\Delta S(z)$ of a single PTCDA molecule as a function of logarithmic distance $\ln(z - z_{\min})$ to a homogeneous substrate.
- fig. S9. Probability ratio from thermodynamic integration and single-molecule simulation as a function of threshold z_0 at $\Delta H_{\text{ads}} = 10k_B T$.
- fig. S10. Additional simulated adsorption of PTCDA on borophene/Ag(111).
- fig. S11. C 1s core-level XPS spectrum of a clean Ag(111) surface.
- fig. S12. Self-assembled PTCDA on Ag(111).
- Legend for movies S1 to S3
- References (49–51)

Other Supplementary Material for this manuscript includes the following:

(available at advances.sciencemag.org/cgi/content/full/3/2/1602356/DC1)

- movie S1 (.avi format). STS maps of homogeneous-phase borophene on Ag(111).
- movie S2 (.avi format). Self-assembly process of PTCDA on heterogeneous borophene/Ag(111) with $\Delta H_{\text{ads,Ag}} = 38k_B T$ and $\Delta H_{\text{ads,B}} = 10k_B T$.

- movie S3 (.avi format). Self-assembly process of PTCDA on heterogeneous borophene/Ag(111) with $\Delta H_{\text{ads,Ag}} = 38k_B T$ and $\Delta H_{\text{ads,B}} = 22k_B T$.

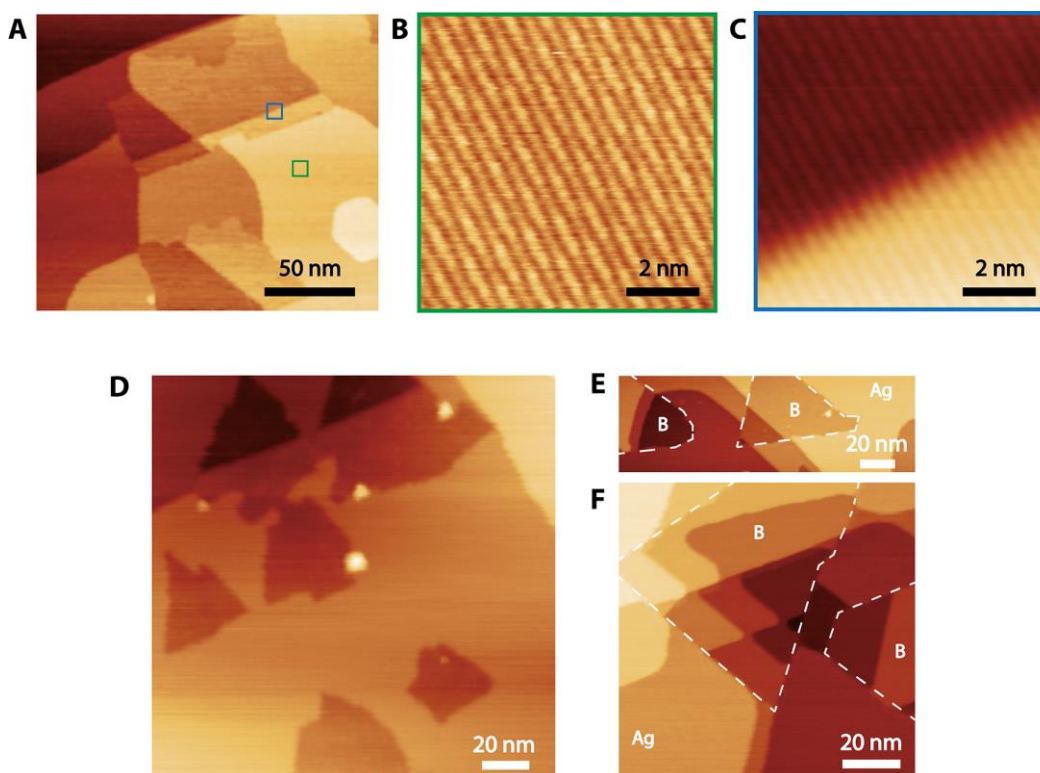


fig. S1. Carpet-mode growth of homogeneous-phase borophene. (A) Scanning tunneling microscopy (STM) image of borophene islands covering Ag(111) step edges ($V_b = 1.5$ V, $I_t = 50$ pA). (B) Atomic resolution STM image of homogeneous-phase borophene growing on a Ag terrace (green square in (A), $V_b = -0.2$ V, $I_t = 50$ pA). (C) STM image of homogeneous-phase borophene continuously growing over a Ag(111) step edge (blue square in (A), $V_b = -0.2$ V, $I_t = 50$ pA). This image confirms that homogeneous-phase borophene adopts carpet-mode growth as has been previously observed for striped-phase borophene (3). (D-F) Additional large-scale STM images of homogeneous-phase borophene growing on and continuously across Ag(111) terraces. The borophene islands in (E) and (F) are outlined by white dashed lines. Ag steps are discontinuous when they cross borophene islands, presumably due to migration of the Ag terraces during borophene growth at elevated temperatures ((D): $V_b = 0.8$ V, $I_t = 50$ pA, (E): $V_b = 1.2$ V, $I_t = 50$ pA, (F): $V_b = 0.91$ V, $I_t = 50$ pA).

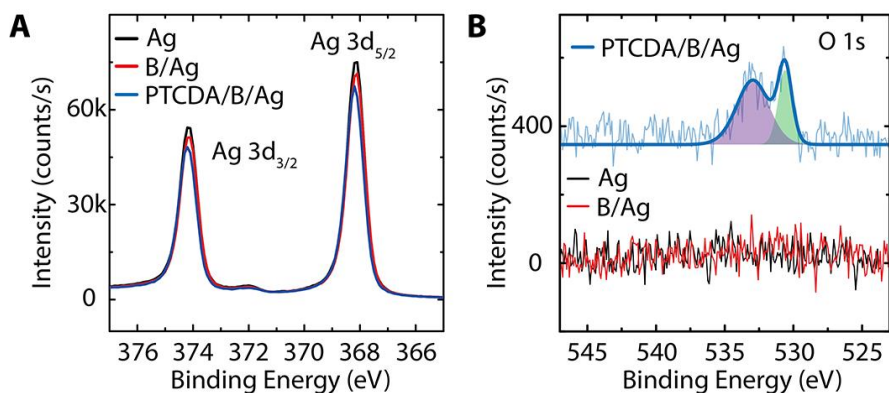


fig. S2. XPS spectra of Ag 3d and O 1s core levels. (A) Ag 3d core-level XPS spectra of clean Ag, borophene/Ag, and PTCDA/borophene/Ag (Ag 3d_{5/2}: 368.2 eV, Ag 3d_{3/2}: 374.2 eV, plasma loss peak of Ag 3d_{5/2}: 372.0 eV (49)). The full widths at half maximum for all three Ag 3d_{5/2} peaks are 0.68 eV. Since the amount of adventitious carbon is small in these samples (fig. S11), all three spectra were charge-corrected by the same amount as determined by the Ag 3d_{5/2} peak position of clean Ag(111). No detectable shift of the peak positions is observed after borophene growth. Following the formation of borophene/PTCDA lateral heterostructures, the Ag 3d_{5/2} is upshifted by 0.04 eV, which is negligible compared to the instrumental energy resolution of 0.6 eV, but could be consistent with a higher binding energy due to electron transfer from Ag to PTCDA as discussed in the main manuscript. (B) O 1s core-level XPS spectra of clean Ag, borophene/Ag, and PTCDA/borophene/Ag (vertically offset). Following PTCDA deposition, two sub-peaks at 530.6 eV and 533.0 eV arise from the C-O-C and C=O bonds in PTCDA (38). The XPS spectra of clean Ag(111) and borophene/Ag(111) show no evidence of oxygen.

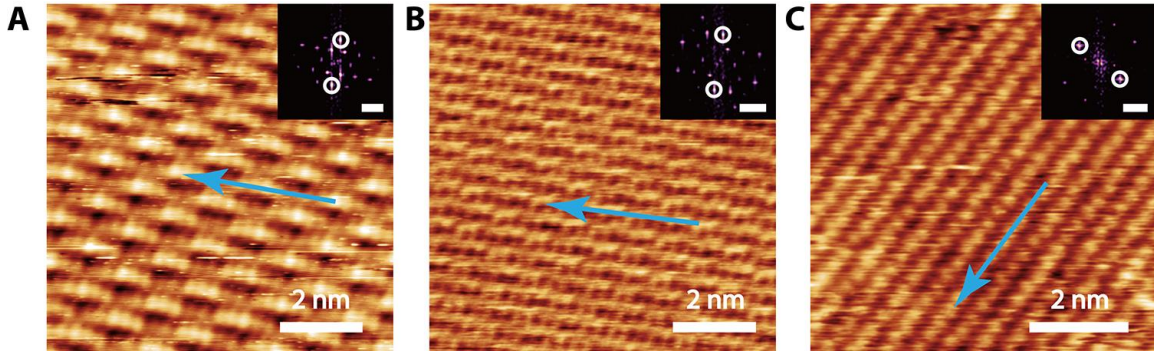


fig. S3. Bias-dependent atomic-resolution images of homogeneous-phase borophene. STM images biasing conditions are (A) $V_b = -1.2$ V, $I_t = 2.36$ nA, (B) $V_b = -0.19$ V, $I_t = 2.36$ nA, (C) $V_b = -0.27$ V, $I_t = 1.45$ nA. The blue arrows indicate the row directions (i.e., the **b** direction in Fig. 2A). Insets: fast Fourier transforms of the corresponding real space images. The scale bars are 2 nm^{-1} . The white circles indicate the frequency-space points that correspond to the periodic row patterns. Although the brick-wall type structure in (A) is commonly observed, finer structure details dominate the contrast at certain scanning conditions, leading to the brick-wall pattern not being discernable, as shown in (B) and (C).

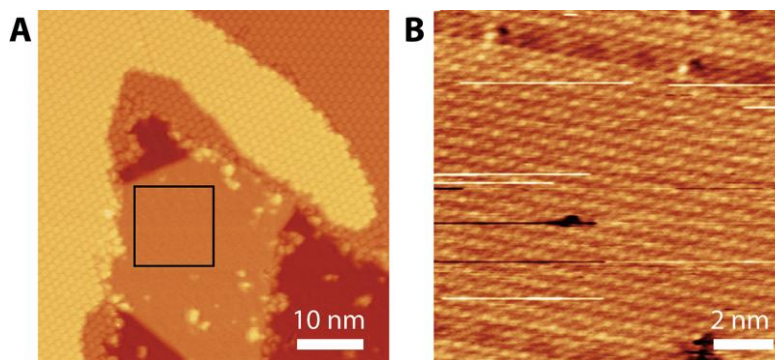


fig. S4. Additional atomic-resolution image of borophene. (A) STM image of the borophene/PTCDA lateral heterostructure in Fig. 3A of the main manuscript ($V_b = -1.7$ V, $I_t = 90$ pA). (B) Atomic resolution image of the borophene region indicated by the black square in (A), supporting the assignment of borophene in Fig. 3A. Line and point defects are seen at the top and bottom parts of the image ($V_b = 0.11$ V, $I_t = 2.54$ nA).

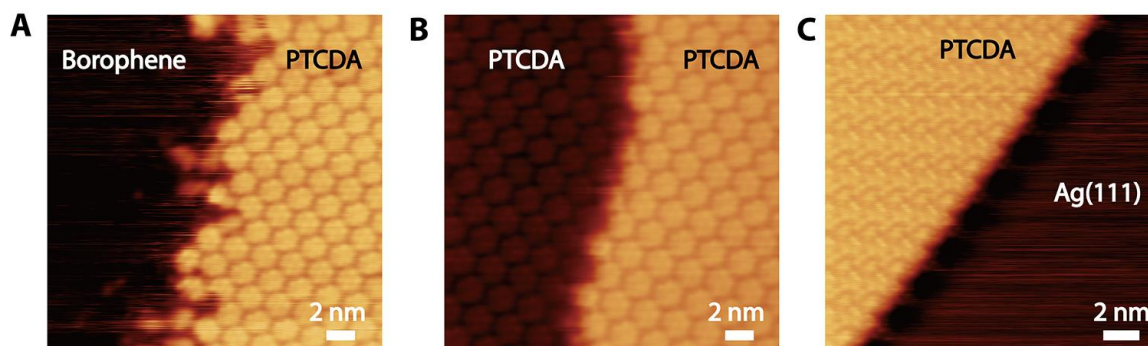


fig. S5. Growth of PTCDA across various interfaces. (A) Borophene/PTCDA interface. The PTCDA molecules are mobile at the interface due to the perturbation of STM tip and the weak interaction between PTCDA and borophene ($V_b = -0.85$ V, $I_t = 60$ pA). (B) Carpet-mode growth of PTCDA across a Ag step edge ($V_b = -0.85$ V, $I_t = 60$ pA). (C) The edge of a PTCDA island on Ag(111) ($V_b = -1.07$ V, $I_t = 50$ pA).

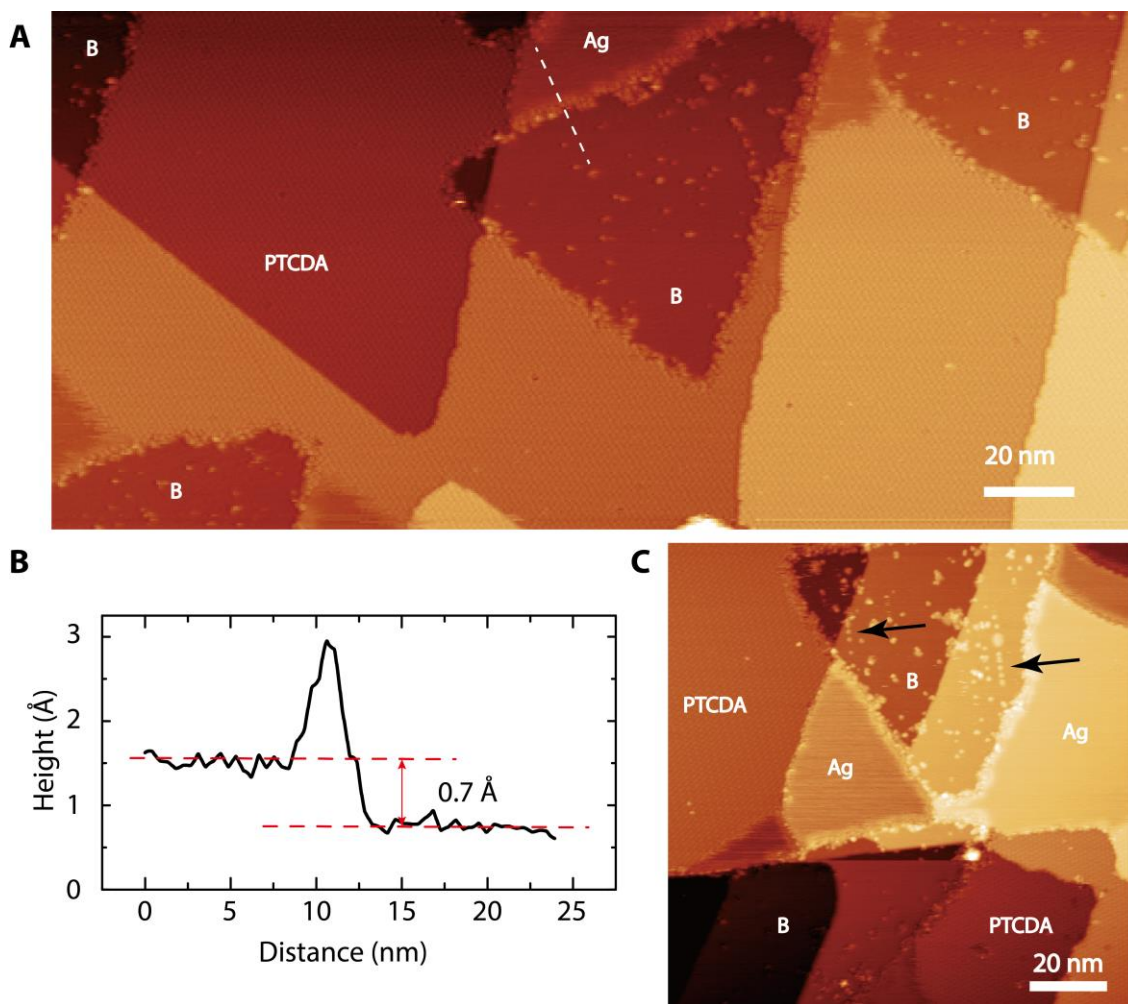


fig. S6. Additional images of PTCDA/borophene lateral heterostructures. (A) Large-scale STM image of borophene islands surrounded by PTCDA monolayers ($V_b = -1.6$ V, $I_t = 50$ pA). (B) The cross-sectional profile along the white dashed line in (A), which reveals the 0.7 Å apparent step height from borophene to Ag(111). (C) The black arrows indicate PTCDA molecules being dragged along the slow scan direction (top to bottom) on borophene, which is consistent with a weak interaction between PTCDA and borophene ($V_b = -1.4$ V, $I_t = 50$ pA).

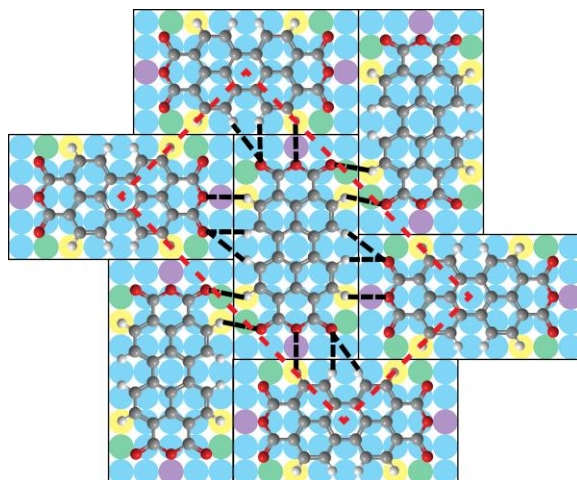


fig. S7. Design of a coarse-grained model for PTCDA. The design is based upon the hydrogen bonding network (48) (black dashed lines) and unit cell (red dashed rectangle) of a self-assembled herringbone lattice. As illustrated, three hydrogen bonds form when the short end of a PTCDA molecule interacts with the side of another molecule. In the PTCDA model, we assign two oxygen beads (purple) at the center of the short sides and four hydrogen beads (yellow) at the long sides, and use the attraction between a pair of oxygen (purple) and hydrogen (yellow) beads to represent the effective interaction resulting from the three hydrogen bonds. Similarly, two hydrogen bonds form when the side of a PTCDA molecule interacts with the side of another molecule. Since this double bond can occur at four sides, we assign another four oxygen beads (green) at the long sides of the molecule, and use the attraction between a pair of oxygen (green) and hydrogen (yellow) beads to represent one hydrogen bond. Thus, the six oxygen beads (green and purple) in the coarse-grained model represent the oxygen atoms in the end groups of a PTCDA molecule, and the four hydrogen beads (yellow) represent the hydrogen atoms at the sides of a PTCDA molecule. The attraction strengths for hydrogen beads with purple oxygen and green oxygen beads are set to $5k_B T$ and $5/3k_B T$, respectively, giving each hydrogen bond strength of $5/3k_B T$, which is within the range of C–H \cdots O hydrogen bond strength (50). The cutoff for the LJ potential is chosen as 4.025 \AA (2.5σ) and shifted to eliminate the discontinuity at the cutoff. All other components in PTCDA molecules interact via purely repulsive LJ potential with cutoff at 1.807 \AA ($2^{1/6}\sigma$, also shifted to eliminate the discontinuity). The electric quadrupole nature of PTCDA (48) makes direct stacking of PTCDA molecules unfavorable, which we

model by placing four virtual beads in the middle of the four sides of a PTCDA molecule. In the simulation, we only aim to probe the effect of heterogeneous substrates on the monolayer growth of PTCDA molecules, thus the virtual bead sizes are chosen to suppress multilayer growth. These virtual beads also account for the repulsive interactions between the negatively polarized anhydride groups of two adjacent molecules, as well as the positively polarized perylene cores of two adjacent molecules (51), which prevent head-to-head and side-by-side assemblies, as experimentally observed. The two virtual beads on the short sides only interact with each other via a purely repulsive LJ potential with $\sigma_1 = 5.796 \text{ \AA}$. Likewise, the two beads on the long sides only interact with each other via the same potential with $\sigma_2 = 6.44 \text{ \AA}$. The interaction strengths are set to $k_B T$ and the interaction cutoffs are set to $2^{1/6}\sigma_1$ and $2^{1/6}\sigma_2$, respectively (shifted to eliminate the discontinuity). The tuning of adsorption enthalpy is achieved by varying the interaction strength between silver atoms and the oxygen and hydrogen beads in PTCDA molecules.

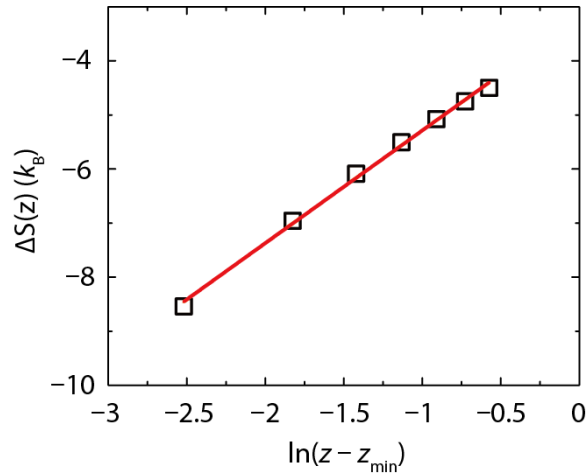


fig. S8. Entropy variation $\Delta S(z)$ of a single PTCDA molecule as a function of logarithmic distance $\ln(z - z_{\min})$ to a homogeneous substrate. z_{\min} is the distance at which the central bead of the PCTDA molecule and a Ag atom are touching. When a PTCDA molecule is in close proximity to the substrate, $\Delta S(z)$ decreases logarithmically with surface separation.

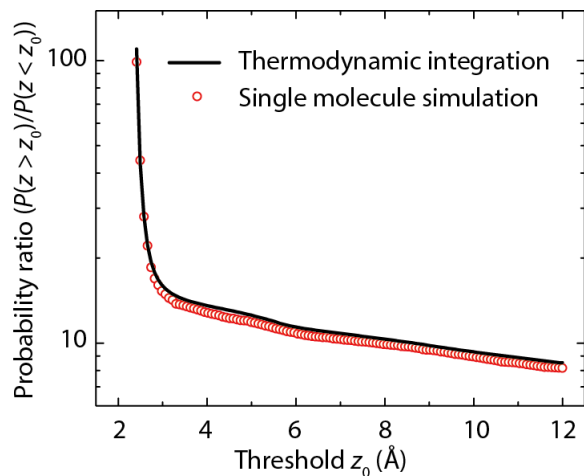


fig. S9. Probability ratio from thermodynamic integration and single-molecule simulation as a function of threshold z_0 at $\Delta H_{\text{ads}} = 10k_{\text{B}}T$. The result from thermodynamic integration is obtained by integrating $\Delta G(z)$

$$\frac{P(z > z_0)}{P(z < z_0)} = \frac{\int_{z_0}^{z_{\text{max}}} e^{-\Delta G(z)} dz}{\int_{z_{\text{min}}}^{z_0} e^{-\Delta G(z)} dz}$$

where z_{min} is the distance at which the central bead of the PCTDA molecule and a Ag atom are touching and z_{max} is the top of the simulation cell. The single-molecule simulation results are obtained by directly sampling the position of a single molecule in a canonical MD simulation. The agreement between the results obtained by direct sampling and thermodynamic integration confirms the calculation of $\Delta G(z)$.

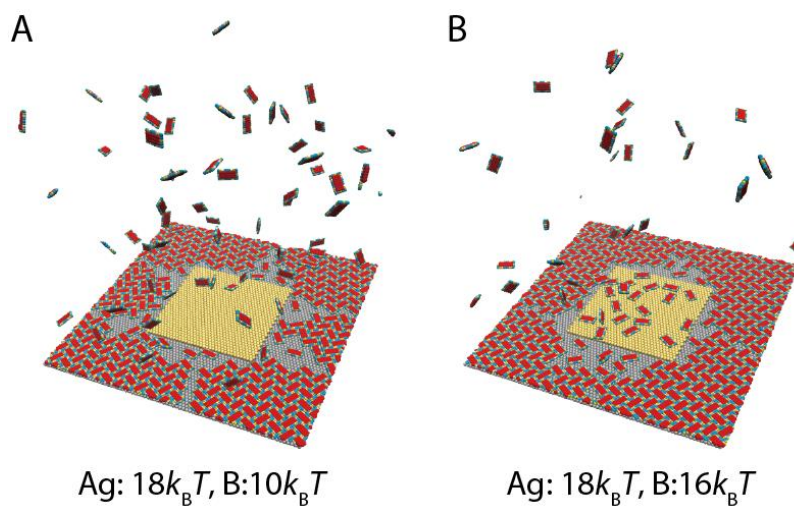


fig. S10. Additional simulated adsorption of PTCDA on borophene/Ag(111). Self-assembled structure of PTCDA on heterogeneous borophene/Ag(111) substrates with (A) $\Delta H_{\text{ads,Ag}} = 18k_B T$, $\Delta H_{\text{ads,B}} = 10k_B T$, and (B) $\Delta H_{\text{ads,Ag}} = 18k_B T$, $\Delta H_{\text{ads,B}} = 16k_B T$. The fact that no PTCDA adsorption is seen in (A) but in (B) indicates that the required adsorption enthalpy differential for PTCDA on Ag(111) and borophene is between 2 and $8k_B T$ for fully selective adsorption of PTCDA on Ag(111).

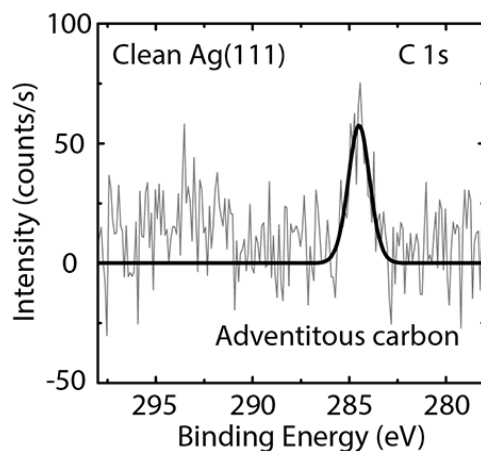


fig. S11. C 1s core-level XPS spectrum of a clean Ag(111) surface. A trace amount of carbon is present (284.5 eV), likely due to adventitious carbon in the ultra-high vacuum chamber.

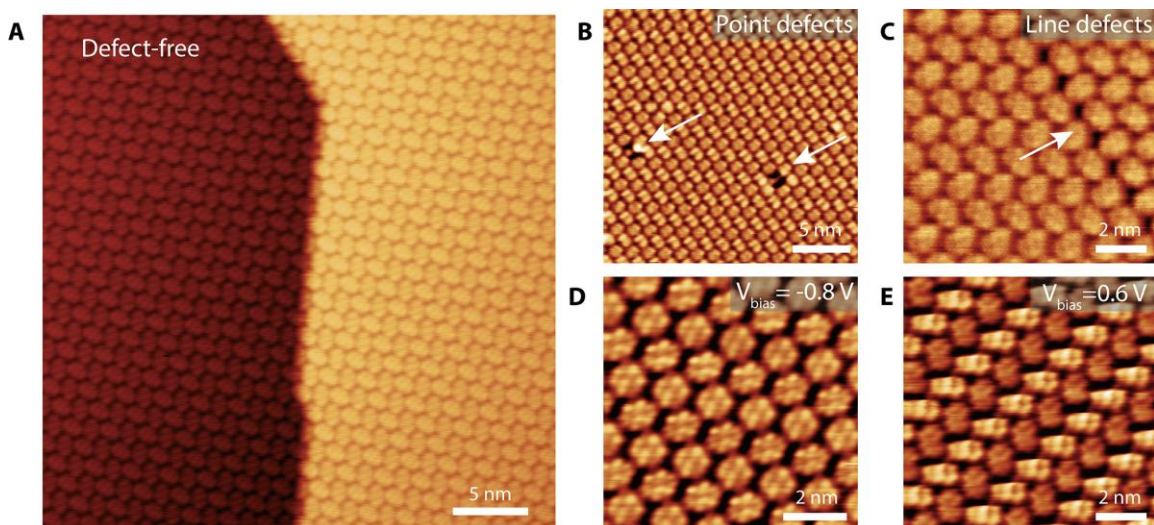


fig. S12. Self-assembled PTCDA on Ag(111). (A) A large area of defect-free PTCDA monolayer showing the herringbone structure across a Ag(111) step edge ($V_b = -0.71 \text{ V}$, $I_t = 50 \text{ pA}$). (B) Point defects ($V_b = -1.07 \text{ V}$, $I_t = 50 \text{ pA}$) and (C) line defects in PTCDA monolayers as indicated by the white arrows ($V_b = -1.75 \text{ V}$, $I_t = 140 \text{ pA}$). (D) STM image of PTCDA imaged at sample bias of -0.8 V and (E) 0.6 V showing different molecular and sub-molecular contrast.

movie S1. STS maps of homogeneous-phase borophene on Ag(111). In the supplementary movie, the STS maps of the borophene island shown in Fig. 2G are shown over a continuous range of biases. The relative dI/dV is color-coded and displayed at each sample bias value (200 voltage values between -0.3 V to 0.7 V) by keeping the differential conductance (dI/dV) of Ag nearly constant. The point spectra of Ag(111) (black) and borophene (red) are also displayed, with the moving blue line indicating the bias voltage. This measurement is performed at room temperature by taking a point STS spectrum (initial tunneling conditions: $V_s = 50$ mV, $I_t = 50$ pA) over a 50×50 grid (8 averages/point) over the course of ~ 5.5 hrs.

movie S2. Self-assembly process of PTCDA on heterogeneous borophene/Ag(111) with $\Delta H_{\text{ads,Ag}} = 38k_B T$ and $\Delta H_{\text{ads,B}} = 10k_B T$. PTCDA molecules preferentially self-assemble on Ag(111).

movie S3. Self-assembly process of PTCDA on heterogeneous borophene/Ag(111) with $\Delta H_{\text{ads,Ag}} = 38k_B T$ and $\Delta H_{\text{ads,B}} = 22k_B T$. PTCDA molecules self-assemble on both Ag(111) and borophene. Even though the adsorption enthalpy differential is $16k_B T$, the large adsorption enthalpy ($22k_B T$) on borophene induces self-assembly of PTCDA.